Journal of Sound and Vibration 417 (2018) 294–305

Contents lists available at ScienceDirect

Journal of Sound and Vibration

journal homepage: www.elsevier.com/locate/jsvi

Matching experimental and three dimensional numerical models for structural vibration problems with uncertainties

P. Langer [a,*], K. Sepahvand [a], C. Guist [b], J. Bär [c], A. Peplow [d], S. Marburg [a]

[a] Chair of Vibroacoustics of Vehicles and Machines, Technical University of Munich, Boltzmann Str. 15, 85748 Garching, Germany
[b] BMW Group, Knorr Str. 147, 80807 Munich, Germany
[c] Institute for Materials Science, Universität der Bundeswehr Munich, Werner-Heisenberg-Weg 39, 85577 Neubiberg, Germany
[d] Department of Natural Sciences and Public Health, Zayed University, P.O. Box 144534, Abu Dhabi, United Arab Emirates

ARTICLE INFO

Article history:
Received 10 August 2017
Revised 24 October 2017
Accepted 21 November 2017
Available online 27 December 2017

Keywords:
Uncertainty quantification
Structural vibration
Experimental modal analysis
Finite element modeling
Parameter identification

ABSTRACT

The simulation model which examines the dynamic behavior of real structures needs to address the impact of uncertainty in both geometry and material parameters. This article investigates three-dimensional finite element models for structural dynamics problems with respect to both model and parameter uncertainties. The parameter uncertainties are determined via laboratory measurements on several beam-like samples. The parameters are then considered as random variables to the finite element model for exploring the uncertainty effects on the quality of the model outputs, i.e. natural frequencies. The accuracy of the output predictions from the model is compared with the experimental results. To this end, the non-contact experimental modal analysis is conducted to identify the natural frequency of the samples. The results show a good agreement compared with experimental data. Furthermore, it is demonstrated that geometrical uncertainties have more influence on the natural frequencies compared to material parameters and material uncertainties are about two times higher than geometrical uncertainties. This gives valuable insights for improving the finite element model due to various parameter ranges required in a modeling process involving uncertainty.

1. Introduction

Accurate modeling and measurement of input parameters is the key to achieving reliable results which determine the dynamic behavior of real structures. Thus, it is essential to clarify the uncertainties involved both in the modeling and measurement process. Uncertainty quantification (UQ) is described as the study of discrepancy between simulation and experimental results [1]. This involves identifying all sources of uncertainty and the solution's sensitivity to these sources. Since the variability of uncertainties for complex structures can be quite pronounced, their quantification involves costly computational efforts making it even unfeasible in most cases. Therefore, defining a simplified model that represents the desired properties of the real structure is crucial. In this regard, simple beam element models are commonly used in finite element method (FEM) studies to quantify the effect of parameter uncertainties, cf. [2–4].

Uncertainties in finite element analysis can be described by many approaches, here we use an interval method (IM) approach. The fundamental aspect to these methods can be found in the literature, cf. [5,6]. General recommendations regarding model

* Corresponding author.
E-mail address: P.Langer@tum.de (P. Langer).

https://doi.org/10.1016/j.jsv.2017.11.042

uncertainties that are important for modeling and for the development process are given in Ref. [7]. These recommendations include valuable ideas: important steps in the model validation process and how to represent results together with their uncertainties. Moore [6] reviewed several interval methods, which can be used to calculate solution limits corresponding to an interval of possible values for experimental results. Sim et al. [8] introduced an efficient modal interval analysis procedure where they identified bounded ranges of parameters and were able to validate the results by comparing them to Monte Carlo simulations. In general, interval arithmetic is a useful tool for describing the propagation of uncertainties for problems when it is not possible to obtain probabilities of different values, Broadwater et al. [9]. Kompella and Bernhard [10] introduced an approach to determine the uncertainty in a production line. Their findings emphasize the importance of uncertainties during production of the final product. They measured the statistical variation of a structural acoustic parameter of vehicles and compared it to a reference measurement value. This method has been applied in various practical engineering problems involving uncertainty and is well-explained in the literature, cf. [11–15]. In acoustics, Hills et al. [16] compared the measurement variability of audio–frequency response of a hatchback model with both a three–door (411 vehicles) and five-door (403 vehicles) derivative and a mid–sized family five-door car (316 vehicles). In summary, the frequency response function (FRF) varied by approximately $5-15$ dB over the frequency range between $0-1000$ Hz for the structure–borne and air–borne paths.

This paper discusses the accuracy of finite element solutions in terms of uncertainties in the model. These uncertainties are divided into two categories: those related to the properties of input parameters (e.g. Young's modulus, density, Poisson's ratio, and dimensions) and those related to the modeling process (approximation due to e.g. discretization or choice of boundary conditions). For characterization, the interval method is employed, see Section 2. The uncertainty of parameters related to material properties is obtained by performing measurements on beam-like steel structures with a parameter identification method described in Section 3.2. The presented ultrasonic measurement of the Young's Modulus E and the error calculation is more accurate than other common methods. Determining the material parameters using inverse modal analysis employing non-destructive identification technique possesses similar accuracy as shown in Refs. [17,18]. To this end, the quantified uncertainties are used as input parameters for the numerical models. These can be divided into one–dimensional or three–dimensional models. In the one–dimensional case, analytical solutions utilizing the Euler–Bernoulli or the Timoshenko beam theory are considered. In the three–dimensional case, a finite element model of the beam-like steel structure is used, utilizing structured hexahedral (brick) elements. Note that beam elements are not considered here because:

(i) their implementation is often based on one of the beam theories which is already covered by taking a one–dimensional model into account and
(ii) they are recommended not to be used in general real world applications, e.g. modeling an engine-transmission unit or a vehicle power train.

By dividing the model uncertainties into different categories and applying the interval method to each of them, the effect of specific uncertainties is presented.

This paper is structured as follows: In Section 2, the theory of interval method and modal analysis are briefly explained. The performed experimental modal analysis is presented in Section 3, whereas the parameter uncertainties and the results from numerical analysis are presented in Section 4. In Section 5, experimental and numerical results are compared. Finally, conclusions are drawn in Section 6. To the best of the authors knowledge this is an original documentation from the application of measured uncertainties, utilization of a finite element model towards a final uncertainty estimation of natural frequencies for a structure. The methods employed here can be easily transformed to real structures such as automobile engine-transmission units.

The following section is important since it shows that in finite element modeling, if the mass and stiffness matrix *uncertainties* are small, the expected uncertainty range for a natural frequency under these deviations due to uncertainty will also be small. In other words the range of uncertainty of one natural frequency is not expected to overlap with the expected range of it's neighbor.

2. Interval stochastic method and modal analysis

Modeling structural beam vibrations is traditionally performed using the lumped model in a single degree–of–freedom (SDOF) or multi degree–of–freedom (MDOF) system. The continuum-based theories employ the Euler-Bernoulli and Timoshenko beam theory in the form of partial differential equations. Detailed descriptions of these theories can be found in the literature [19,20]. Additionally, the finite element method can be employed to analyze the structural beam vibrations employing different finite elements, cf. [21–26] for instance. Regarding uncertainties, the stochastic finite element modeling uses various probabilistic and possibilistic methods. Among them, the interval stochastic method is chosen for the analysis of the beam-like structure because of its straightforward application. The applied interval operations and the performed interval-based stochastic modal analysis is briefly presented in the following. For an in–depth introduction to interval methods refer to Qiu et al. [27].

Assuming real numbers $\mathbb{R}$, a closed interval X^{I} is defined by

$$X^{\mathrm{I}} = [x_{\min}, x_{\max}] = \left\{ x \in \mathbb{R} | x_{\min} \leq x \leq x_{\max} \right\}, \qquad x_{\min}, x_{\max} \in \mathbb{R}, \tag{1}$$

with lower limit $x_{\min}$ and upper limit $x_{\max}$. By defining X^{A} as average value of X^{I} and ΔX as maximum width or radius of X^{I}, i.e.

$$X^A = \frac{x_{\min} + x_{\max}}{2}, \quad \Delta X = \frac{x_{\max} - x_{\min}}{2}. \tag{2}$$

Eq. (1) can be transformed into

$$X^I = \left[X^{\mathrm{A}} - \Delta X,\ X^{\mathrm{A}} + \Delta X\right]. \tag{3}$$

Removing X^{A} out of the interval yields:

$$X^{\mathrm{I}} = X^{\mathrm{A}} + \Delta X^{\mathrm{I}}, \quad \Delta X^{\mathrm{I}} = [-\Delta X, \Delta X], \tag{4}$$

with ΔX^{I} representing the radius of uncertainty. In the same way an $n \times n$ interval matrix $\mathbf{H}$ can be described according Sim et al. [8]. Basically, this involves creating intervals for each entry, $\mathbf{H}_{\mathrm{ij}}$, in the matrix.
For an undamped free vibration problem with n degrees of freedom, the equations of motion in matrix notation read

$$\mathbf{M}\ddot{\mathbf{y}} + \mathbf{K}\mathbf{y} = \mathbf{0}, \tag{5}$$

with $\mathbf{M}$ and $\mathbf{K}$ being real, positive semi-definite $n \times n$ matrices for mass and stiffness, respectively, as well as $\mathbf{y}$ and $\ddot{\mathbf{y}}$ representing the vectors of displacement and acceleration, respectively. Assuming that $\mathbf{y}$ features a time-dependency of $e^{i\omega t}$, the separation of variables yields

$$\mathbf{y}(\mathbf{t}) = \hat{\mathbf{y}}e^{i\omega t}, \quad \ddot{\mathbf{y}} = -\omega^2\hat{\mathbf{y}}e^{i\omega t}. \tag{6}$$

Hence the eigenvalue problem can be written as

$$\left(\mathbf{K} - \omega^2\mathbf{M}\right)\hat{\mathbf{y}} = \mathbf{0}, \tag{7}$$

which are the undamped system's eigenfrequencies ω, and $\hat{\mathbf{y}}$ contains the eigenvector components. For symmetric systems, the eigenvalues can be extracted using the Lanczos method as described in Refs. [28,29] or, in case of finite element applications, employing the method described by Bathe and Wilson [30].

Taking uncertainties into account, both mass and stiffness matrix uncertainties are rewritten as:

$$\mathbf{K}^{\mathrm{I}} = \mathbf{K}^{\mathrm{A}} + \Delta\mathbf{K}^{\mathrm{I}}, \quad \Delta\mathbf{K}^{\mathrm{I}} = -\Delta\mathbf{K}, \Delta\mathbf{K}, \tag{8}$$

$$\mathbf{M}^{\mathrm{I}} = \mathbf{M}^{\mathrm{A}} + \Delta\mathbf{M}^{\mathrm{I}}, \quad \Delta\mathbf{M}^{\mathrm{I}} = -\Delta\mathbf{M}, \Delta\mathbf{M}. \tag{9}$$

Substituting these into the eigenvalue problem of Eq. (7) yields the same problem, but in interval notation

$$(\mathbf{K}^{\mathrm{I}} - \omega^2\mathbf{M}^{\mathrm{I}})\hat{\mathbf{y}} = \mathbf{0}. \tag{10}$$

The undamped system's circular frequencies ω^2 are the square roots of the characteristic polynomial, i.e.

$$\det\left(\left(\mathbf{K}^{\mathrm{A}} + \Delta\mathbf{K}^{\mathrm{I}}\right) - \omega^2\left(\mathbf{M}^{\mathrm{A}} + \Delta\mathbf{M}^{\mathrm{I}}\right)\right) = 0. \tag{11}$$

Herein, $\mathbf{K}^{\mathrm{A}}$ and $\mathbf{M}^{\mathrm{A}}$ are the nominal values for the stiffness and mass matrix, respectively, with $\Delta\mathbf{K}^{\mathrm{I}}$ and $\Delta\mathbf{M}^{\mathrm{I}}$ being their associated uncertainties. Each interval is limited by corresponding bounds as defined in Eq. (1).

The interval method yields two natural frequency limits $f_{\mathrm{i}_{\min}}$ and $f_{\mathrm{i}_{\max}}$ obtained for the first bending modes of the beam–like structure. These two values represent the bounds of the interval in which the natural frequency of a certain modes lie, depending on the corresponding uncertainties. Hence, the system's circular frequencies of the i-th bending mode must lie in the interval

$$\omega^2{}_{\mathrm{i}} = [\omega^2{}_{\min},\ \omega^2{}_{\max}] = \left[\frac{\phi^T\underline{\mathbf{K}}\phi}{\phi^T\overline{\mathbf{M}}\phi}, \frac{\phi^T\overline{\mathbf{K}}\phi}{\phi^T\underline{\mathbf{M}}\phi}\right] \tag{12}$$

for which the natural frequency intervals, f^{I} can be found. Herein, ϕ is the modal matrix which consist of the eigenvectors, ϕ^T is the matrix transpose of ϕ and the over- and underlined matrices $\mathbf{K}, \mathbf{M}$ represent the upper and lower values due the corresponding uncertainties, respectively.

3. Model description and experiments

For the experimental analysis, ten distinct beam-like structures with nominal dimensions length $l = 0.2$ m, width $w = 0.04$ m and height $h = 0.004$ m are considered, cf. Fig. 1(a). The specimens' manufacturing tolerances match DIN ISO 2768-1 (m), which is the common standard in the automotive industry, e.g. the same tolerances as applied on a production line. Therefore, the dimensions including tolerances are given by $l = 0.2$ m $\pm$ 0.0005 m, $w = 0.04$ m $\pm$ 0.0003 m and $h = 0.004$ m $\pm$ 0.0001 m. The specimens were made of steel, for which linear elastic material behavior, i.e. Hooke's Law, is assumed. The experimental determination of the material properties is described in Section 3.2, whereas the next section describes the performed experimental modal analysis. The natural frequencies of the first three bending modes are determined through EMA of each specimen. Fig. 1(b) shows a three–dimensional finite element model of the beam-like structure with a mesh built from of 20–node quadratic brick elements.

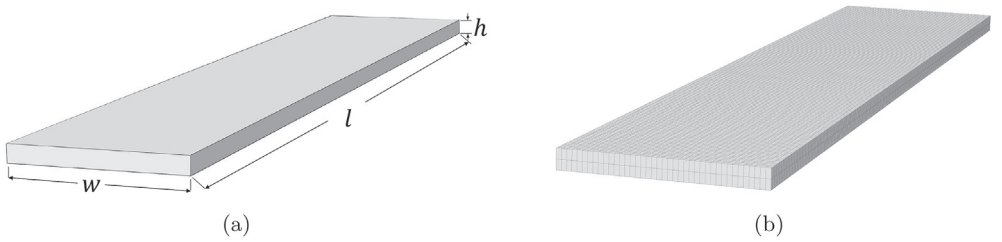

Fig. 1. Investigated models. (a) Beam-like structure; nominal values: $l = 0.2$ m, $w = 0.04$ m and $h = 0.004$ m. (b) Three–dimensional finite element model of the beam-like structure with an efficient mesh.

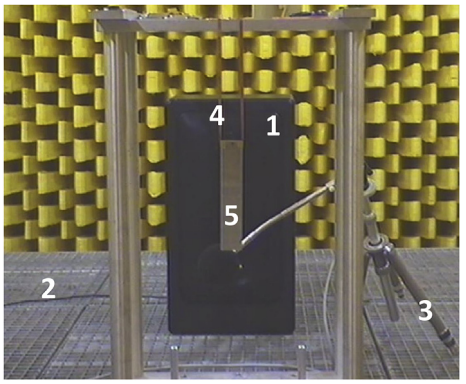

Fig. 2. Experimental setup of beam-like structure: (1) loudspeaker; (2) anechoic chamber; (3) microphone; (4) elastic strings; (5) specimen.

3.1. Experimental modal analysis (EMA)

By performing an experimental modal analysis, it makes evaluation of modal parameters based on measured frequency response functions a reality. The modal parameters, such as eigenfrequencies, modal damping, and eigenvectors can be evaluated numerically using a curve–fitting algorithm together with a decomposition scheme of the fitted polynomials. In this paper, the impact of parameter uncertainty on the value of eigenfrequencies of a beam-like structure is investigated.

In an experimental modal analysis, the accuracy of the measurement is highly dependent on the precision of the measuring device and setup. Therefore, a suitable measurement technique is required to accurately record the excitation and the structural response. In order to examine the beam-like specimen, the structure is excited with a loudspeaker and the sound pressure is measured between the loudspeaker and the specimen. Note that this method is only applicable for lightweight sound-sensitive structures. This means the structures can be excited by acoustic means, such as loudspeakers. Various standard measurement techniques have been recommended in Ewins [31] and ISO 7626-1:2011 [32].

In all experiments, free–free boundary conditions were considered to match the simple simulation models. This is an idealization of the real setup. However, since the frequency of the corresponding rigid body motions was an order of magnitude smaller than the frequency of the first deflection shape, the influence of the boundary conditions on the first resonance frequency was disregarded. In the experimental setup, the structure was attached to two elastic strings in an anechoic chamber, Fig. 2 and a microphone measured the sound pressure level in front of the loudspeaker, which excited the structure with a periodic chirp signal. Two major advantages of the this excitation signal are, first, its continuity up to the first derivative, and second, its periodicity within the time block. Therefore, a continuous and sequential measurement is possible using a scanning laser Doppler vibrometer. Time signals of all quantities are transferred into the frequency domain using Fast Fourier Transformation (FFT) and are further processed to obtain the FRF for each measurement. Eigenfrequencies and associated mode shapes are identified by processing the FRFs with the post-processing tool ME'scope.

3.2. Experimental parameter identification method

The material parameters, namely Young's modulus E and Poisson's ratio ν are determined using ultrasonic measurements [33,34]. The sound velocity of longitudinal (c_l) and transversal (c_t) waves in an elastic continuum are given by

$$c_l = \sqrt{\frac{E(1-\nu)}{\rho(1+\nu)(1-2\nu)}} \tag{13}$$

and

$$c_t = \sqrt{\frac{E}{2\varrho(1+\nu)}}, \tag{14}$$

respectively. Herein, ϱ denotes the structure's density. Transforming both equations yields two expressions for Young's modulus E, i.e.

$$E(c_l) = \frac{{c_l}^2\varrho(1+\nu)(1-2\nu)}{(1-\nu)} \tag{15}$$

and

$$E(c_t) = 2{c_t}^2\varrho(1+\nu). \tag{16}$$

Assuming that $E(c_l) = E(c_t)$ results in

$$\nu = \frac{2{c_t}^2 - {c_l}^2}{2({c_t}^2 - {c_l}^2)}. \tag{17}$$

Given the longitudinal and transversal wave velocities c_l and c_t, Poisson's ratio ν can be easily obtained from Eq. (17) For determining the Young's modulus, Eqs. (15) and (16) are evaluated and their results averaged, i.e. $E = 1/2\ (E(c_l) + E(c_t))$. The differences between $E(c_l)$ and $E(c_t)$ are negligible since these are lower than the calculated uncertainties. Therefore, the changes of the uncertainty according to Eq. (22) is also negligibly small. The averaging is therefore not necessary, but it is performed to eliminate small errors. The ultrasonic measurements are performed using the 5 MHz ultrasonic module UT/Mate from Vogt ultrasonics and transducers. All measurements are taken in reflection mode, i.e. pulse–echo mode, on specimens with plane-parallel grinded surfaces. On each specimen, ten individual measurements are taken for both longitudinal and transversal sound velocities.

The density is measured employing hydrostatic weighing via Archimedes' principle. For this, an analytical balance Mettler Toledo 204AG of 0.1×10^{-3} g scale is used. Each specimen was first weighed in air yielding m_{air} and then weighed in water yielding m_{water}. Given the two masses and the density of water ϱ_{water} and air ϱ_{air}, the density ϱ of the specimen can be calculated using Eq. (18) without knowledge of the specimen's volume.

$$\varrho = \frac{m_{\text{air}}(\varrho_{\text{water}} - \varrho_{\text{air}})}{m_{\text{air}} - m_{\text{water}}} + \varrho_{\text{air}} \tag{18}$$

Having the experimental setup, the next step is to quantify the total measurement uncertainty. In general, the uncertainty consists of systematic and random errors. The systematic errors result from the deviation of the measurement equipment and the random errors are based on the measurements' standard deviation.

Regarding the error calculation of Poisson's ratio, Young's modulus, and density, the Gaussian error propagation is applied. Within the Gaussian error propagation, the error of a given parameter p depending on independent variables $x_1, x_2, \ldots, x_n$ is given by

$$\Delta p = \left[\sum_{i=1}^{n}\left(\frac{dp}{dx_i}\Delta x_i\right)^2\right]^{\frac{1}{2}}. \tag{19}$$

Accordingly, the error propagation of the density in Eq. (18) is calculated as

$$\Delta\varrho = \left[\left(\frac{d\varrho}{d\varrho_{\text{water}}}\Delta\varrho_{\text{water}}\right)^2 + \left(\frac{d\varrho}{d\varrho_{\text{air}}}\Delta\varrho_{\text{air}}\right)^2 + \left(\frac{d\varrho}{dm_{\text{air}}}\Delta m_{\text{air}}\right)^2 + \left(\frac{d\varrho}{dm_{\text{water}}}\Delta m_{\text{water}}\right)^2\right]^{\frac{1}{2}}. \tag{20}$$

with the uncertainties being $\Delta m_{\text{air}} = 0.1 \times 10^{-3}$ g, $\Delta m_{\text{water}} = 1 \times 10^{-3}$ g, $\Delta\varrho_{\text{air}} = 2.95 \times 10^{-6}$ gcm^{-3}, and $\Delta\varrho_{\text{water}} = 0.001$ gcm^{-3}. The uncertainties for weighing in air Δm_{air} corresponds to the resolution of the scale from the Mettler Toledo 204 AG equipment. For weighing in water Δm_{water}, due to the higher level of difficulty of this measurement, a higher uncertainty was expected. The values of the uncertainty were proven by checking against several measurements. The values of $\Delta\varrho_{\text{air}}$ and $\Delta\varrho_{\text{water}}$ correspond to a change in temperature of 1.5 Kelvin. The error propagation of Poisson's ratio is given as

$$\Delta\nu = \left[\left(\frac{c_t{c_l}^2}{({c_t}^2 - {c_l}^2)^2}\Delta c_t\right)^2 + \left(\frac{c_l{c_t}^2}{({c_l}^2 - {c_t}^2)^2}\Delta c_l\right)^2\right]^{\frac{1}{2}}, \tag{21}$$

with the measurement uncertainty of $\Delta c_l = \Delta c_t = 50$ m/s. Regarding the error propagation of the Young's modulus, it is repeated that $E = 1/2\ (E(c_l) + E(c_t))$. Thus the error propagation is split into two parts, i.e.

$$\Delta E = \left[\left(\frac{1}{2}\Delta E(c_l)\right)^2 + \left(\frac{1}{2}\Delta E(c_t)\right)^2\right]^{\frac{1}{2}}. \tag{22}$$

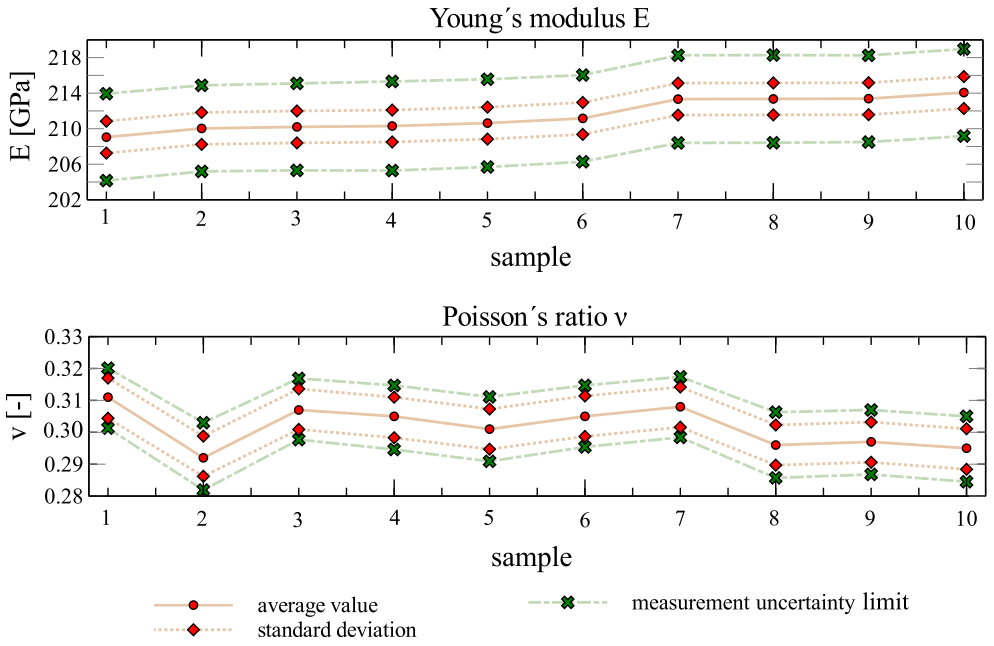

Fig. 3. Average value, standard deviation, and measurement uncertainty for Young's modulus E and Poisson's ratio ν for ten beam-like samples.

With respect to Eqs. (15) and (16), these read

$$\Delta E(c_l) = \left[\left(\frac{2c_l\rho(1+\nu)(1-2\nu)}{(1-\nu)} \Delta c_l \right)^2 + \left(\frac{v_l^2(1+\nu)(1-2\nu)}{(1-\nu)} \Delta\rho \right)^2 + \left(\frac{2v_l^2\rho\nu(\nu-2)}{(1-\nu)^2} \Delta\nu \right)^2 \right]^{\frac{1}{2}}, \tag{23}$$

and

$$\Delta E(c_t) = \left[\left(4c_t\rho(1+\nu)\Delta c_t\right)^2 + (2c_t^2(1+\nu)\Delta\rho)^2 + (2c_t^2\rho\Delta\nu)^2 \right]^{\frac{1}{2}}. \tag{24}$$

Based on the performed experiments and the stated error propagations, Fig. 3 shows average values, standard deviations, and uncertainties of Poisson's ratio and Young's modulus for each specimen. These measurement uncertainties then requires to consider input parameters in the finite element analysis as uncertain.

In addition, Fig. 4 shows the average value and the measurement uncertainty of the specimens' geometry, i.e. their length l, width w, and height h. These measurements have been collected three times at three different positions of the specimens. For instance, to measure the height h of the specimen, three measurements were taken at $l = 0.01$ m, 0.1 m, and 0.19 m. Hence, the determined height h is an average value of nine measurements in total. The shown measurement uncertainty directly results from the accuracy of the measuring instrument and takes the value $\pm 0.02 \times 10^{-3}$ m. The averaged measurement uncertainty of Young's modulus and Poisson's ratio are shown in Fig. 3 are $\pm 2.3\%$ and $\pm 3.2\%$, respectively. Furthermore, the average density of the specimens equals 7.817 gcm^{-3} with an averaged measurement uncertainty $\pm 0.171\%$.

As mentioned previously, both the averaged values and the measurement uncertainties are used as input parameters to the finite element analysis.

4. Efficient finite element modeling

In this section, a guideline on constructing efficient and accurate numerical models is given based on the beam-like steel structure. In this context, two well known analytical beam theories, Euler-Bernoulli and Timoshenko, are considered together with a finite element model. The guideline reads as follows:

(a) defining physical dynamic behavior of the structure,
(b) identifying uncertainties,
(c) analyzing sensitivities,
(d) identifying irrelevant uncertainties,
(e) finding a compromise between accuracy and computational effort of the numerical model.

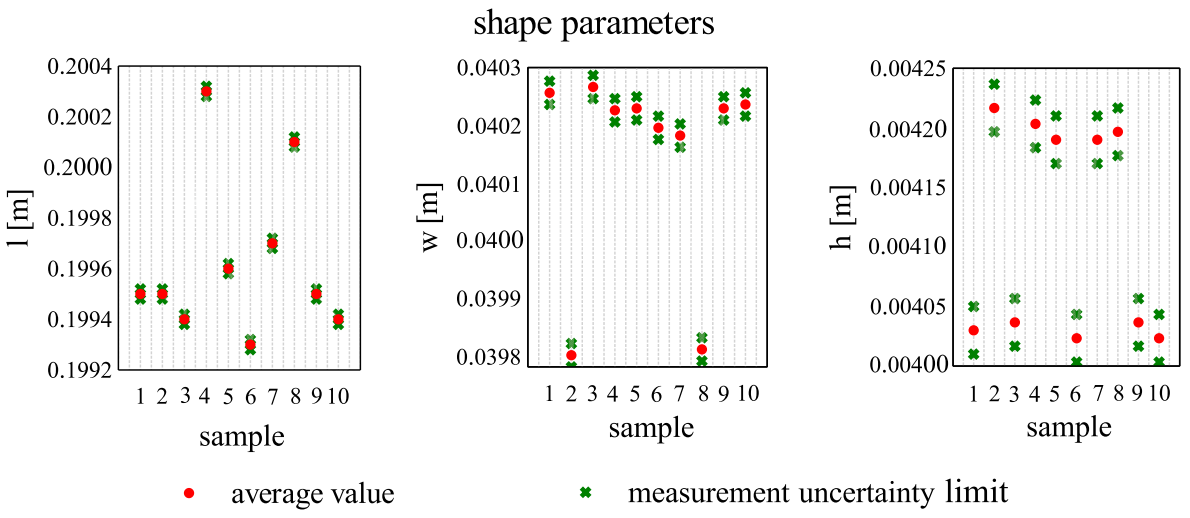

Fig. 4. Dimensions in terms of the average value and measurement uncertainty of ten beam-like samples for the length l, the width w, and the height h.

In the following, these aspects will be discussed in more detail. Steps (b) to (e) will be discussed from two different viewpoints: uncertainties in geometrical and material parameters and uncertainties in the modeling process, i.e. due to discretization and modeling assumptions.

4.1. Defining physical dynamic behavior of the structure

The physical behavior of a beam-like structure depends on material and geometrical parameters, structural damping, and boundary conditions. The material parameters include Young's modulus E, the density ϱ and Poisson's ratio ν. The essential geometrical parameters are the length l, the width w, and the height h of the structure. Regarding the structural damping, its effect is assumed to be small and thus damping is neglected within this investigation. The boundary conditions, which are discussed in Section 3.1, are idealized as free-free boundary conditions so that the corresponding uncertainty is neglected here.

4.2. Identifying uncertainties

4.2.1. Uncertainties in material and geometrical parameters

The uncertainties of both material and geometrical parameters have already been discussed in Section 3.2. Following the notation of Eq. (1), the uncertainty intervals are given by

$$E^{\mathrm{I}} = [E_{\min}, E_{\max}] \quad \varrho^{\mathrm{I}} = [\varrho_{\min}, \varrho_{\max}] \quad \nu^{\mathrm{I}} = [\nu_{\min}, \nu_{\max}] \tag{25}$$

$$l^{\mathrm{I}} = [l_{\min}, l_{\max}] \qquad w^{\mathrm{I}} = [w_{\min}, w_{\max}] \quad h^{\mathrm{I}} = [h_{\min}, h_{\max}] \tag{26}$$

Other uncertainties are neglected, e.g. uncertainties in the straightness and flatness, surface roughness, and angle perpendicularity of the beam-like structure.

4.2.2. Uncertainties in the numerical modeling process

The physical behavior of general structures is described by partial differential equations for which analytical solutions seldom exist. Under certain conditions, the observed structure or its physical behavior can be idealized. For beam-like structures, several beam theories allowing a description in simplified partial differential equations (PDE) exist. The accuracy of the solution depends greatly on these assumptions. Two well-known given model assumptions, Euler-Bernoulli and Timoshenko beam theories, are investigated. The Euler–Bernoulli beam theory assumes no shear deflection and rotary inertia. For this reason the Timoshenko theory is formulated to cover this drawback. First, the shear stress distribution across the cross section is assumed to be constant and linear. Second, the cross–sectional area is assumed to be symmetric so that the neutral and centroidal axes coincide. A comprehensive study on various beam theories is given in Ref. [19]. But it is generally assumed that the Timoshenko theory possesses greater accuracy due to it's advanced underlying formulation.

For real-life, general structures it is often valuable to revert to solving the underlying PDE via the finite element method. Within the numerically based FEM, an exact solution can be only be found if the discretization and the chosen shape functions are able to represent the exact solution. In real-world problems this is almost never the case. Errors arise due to the chosen

discretization of the structure and the weak formulation of the Galerkin method. In the present context, the idealized free–free boundary conditions additionally introduce an error relative to the way that the beam-like structures are suspended in the measurement setup. Another error is introduced by neglecting structural damping in the numerical modeling process.

Uncertainties arising due to model assumptions and the mesh discretization are not easily quantified. However, their effect can be determined by comparing the numerical results with a reference solution. This is shown in the following section.

4.3. Analyzing sensitivities

In the sensitivity analysis, the numerical results are compared with a reference solution. Here, the comparative quantity is a natural frequency f identified with an object, as discussed in Section 2. Regarding the one–dimensional models, the reference natural frequency is denoted by f_N ($k = \mathrm{N}$), which is determined by a finite element analysis using mean values for geometrical and material parameters. The corresponding relative deviation reads

$$\varepsilon_k = \frac{1}{m}\sum_{i=1}^{m}\left(\frac{f_{k_\mathrm{i}}}{f_{\mathrm{N_i}}} - 1\right) \times 100, \qquad k = \mathrm{T}, \mathrm{B}, \tag{27}$$

with the natural frequencies f_B and f_T being determined employing the Euler–Bernoulli ($k = \mathrm{B}$) and Timoshenko ($k = \mathrm{T}$) beam theory, respectively. Regarding the finite element results, the reference natural frequency denoted by f_{LDV} is determined by performing experimental modal analysis over ten specimens and averaging the results. For the finite element results, the relative deviation is given by

$$\varepsilon_k = \frac{1}{m}\sum_{i=1}^{m}\left(\frac{f_{k_\mathrm{i}}}{f_{\mathrm{LDV_i}}} - 1\right) \times 100, \qquad k = \mathrm{N}, \mathrm{M}, \mathrm{S}. \tag{28}$$

Herein, f_M represents the natural frequencies' upper limit when using mean values of the geometrical parameters, but lower and/or upper limits of the material parameters ($k = \mathrm{M}$). In contrast, f_S represents the natural frequencies' upper limit when using mean values of the material parameters, but lower and/or upper limits of the geometrical parameters. To determine f_S for instance, the lower limit of length l and the upper limit of height h and width w is chosen ($k = \mathrm{S}$). The possibility that a combination of material and geometrical parameters not being upper or lower limits yields a higher upper limit of the natural frequency has been neglected. Having defined different references in Eqs. (27) and (28) allows quantifying the relative deviation which arises from the discretization employed in the finite element model.

In Fig. 5, the relative deviations are shown for the first three bending modes. Note that the deviation is expressed in the height of the bars and their position, i.e. above or below the abscissa and not in the distance to the abscissa. To begin with, the focus is set on the deviation due to the model assumptions of Euler–Bernoulli and Timoshenko beam theory, ε_B and ε_T, respectively. While ε_B is of equivalent size for all three bending modes, ε_T significantly increases with the mode order. Since Timoshenko beam theory extends the Euler–Bernoulli theory by additional shear deformations, the resulting reduced stiffness yields lower natural frequencies. Both ε_B and ε_T underestimate the natural frequency in all bending modes except the first, where ε_B is positive. For an in-depth analysis of beam theories, see Labuschagne et al. [35]. Now, consider ε_D, the deviation due to the discretization of the finite element model. With a relative deviation below 0.1%, the finite element model simulates the experimental setup very well, using mean values for both geometrical and material parameters. The deviation is of similar size as ε_B which underestimates the natural frequency as well. The small relative deviation additionally shows that the idealized free–free boundary conditions and the effect of gravity is very low. For a more detailed analysis of different mesh densities, c.f. Langer et al. [36]. Further comparing ε_D to both ε_M and ε_S clearly emphasizes the effect of both material and geometrical uncertainties: The relative deviations are 5 to 20 times higher. Although different reference values are used, it is not ambiguous that in this case the effect of material and geometrical uncertainties is significantly higher than the impact of the assumptions made by the Euler–Bernoulli beam theory. Similar to ε_D, both ε_M and ε_S are of nearly equal size for all three bending modes. Regarding their size, the material uncertainties have a greater impact than the geometrical uncertainties. The relative deviation depends heavily on the width of the uncertainty interval, this is restricted to the present case. Although the geometrical uncertainty interval is about 10 to 100 times smaller compared to the material uncertainty interval, Section 3.2, the relative deviation only differs by a factor of just over 2.

4.4. Disregarding irrelevant uncertainties

With the outcome of the sensitivity analysis known, small or even irrelevant uncertainties might be disregarded.

4.4.1. Uncertainties in material and geometrical parameters

As demonstrated in the last section, the determined uncertainties of both material and geometrical parameters should be included in the numerical models. Even small errors in these parameters have a significant influence on the model's results. A statement towards the already neglected uncertainties, e.g. straightness and flatness, surface roughness, and angle perpendicularity of the beam-like structures however is not possible.

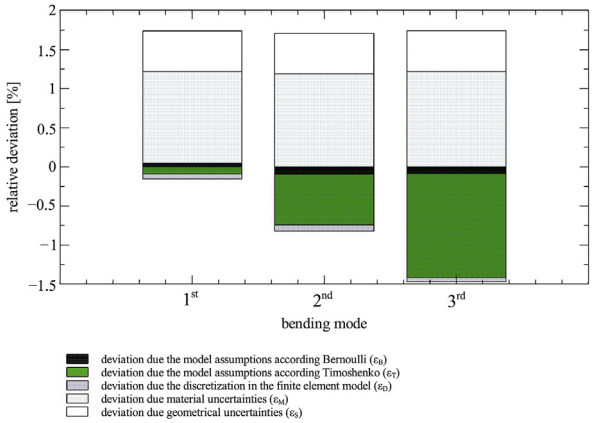

Fig. 5. Relative deviation arithmetically averaged over 10 samples for bending modes compared to an idealized model for the first three eigenfrequencies. Note that the deviation is expressed in the height of the bars and their position, i.e. above or below the abscissa and not by the distance to the abscissa.

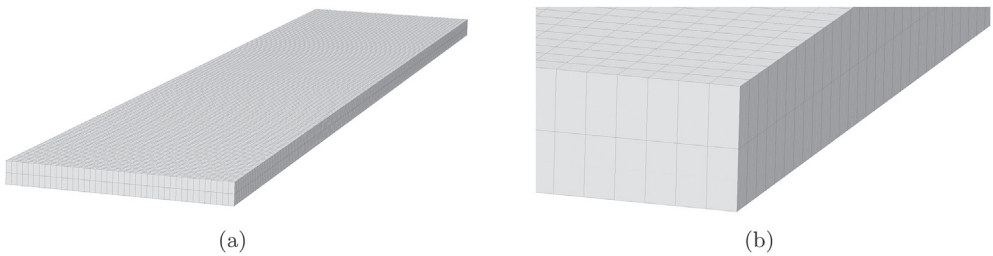

Fig. 6. Defined finite element model with the most efficient mesh. (a) Finite element model; (b) magnified view.

4.4.2. Uncertainties in the numerical modeling process

Having determined a small relative deviation between the finite element model using mean parameter values and the experimental modal analysis, it is assumed that the uncertainty arising from the idealized free–free boundary condition and gravity are negligible. A similar argument holds for the structural damping, since damping was not taken into account in the first place.

4.5. Computational accuracy vs. effort

In numerical analyses, there is often a trade off between the achievable accuracy and the available computing time. In this case, the discussion in step (c), Section 4 shows that a model based on the Timoshenko beam theory is not accurate enough although more computationally efficient. In contrast, the Euler–Bernoulli beam theory tends to provide more accurate results while being computational efficient. In finite element models, the solution's quality is mainly determined by the chosen discretization and shape functions. In a recent study a finite element analyses of the same beam-like structure were performed by Langer et al. [37] using different discretizations and shape functions. A convergence study using over five times the number of degrees of freedom as those used here, showed that an improvement of less than 0.5% was achieved when calculating the natural frequencies of the first three bending modes. The finite element discretization used here is a compromise found in Refs. [37,38] between computational accuracy and computational effort. Using this discretization, a model with two-layers of 20–node quadratic brick elements and an element edge length of 1 mm is used. This equals a total number of 1.6×10^4 elements and 2.7×10^5 degrees of freedom. After consideration of points (a)–(e), the finite element model with the most efficient mesh was chosen, as shown in Fig. 6.

5. Comparison with experimental results

In this section, a comparison between experimental and numerical results is presented for each of the ten beam-like specimens. This includes results of analytical models based on Euler–Bernoulli and Timoshenko theory, including results from finite element models. Again, the comparative quantities are the natural frequencies of the first three bending modes and their corresponding uncertainty. However this time, for each of the ten physical beam-like structures three–dimensional numerical models were assembled. Regarding the models' input, both material and geometry parameters are used including their corresponding uncertainties, as presented in Section 3.2. For comparison reasons, an uncertainty of $\pm 1\%$ is assumed for the experimentally determined natural frequencies. This is an empirical value which includes the uncertainties of the measurement setup, signal

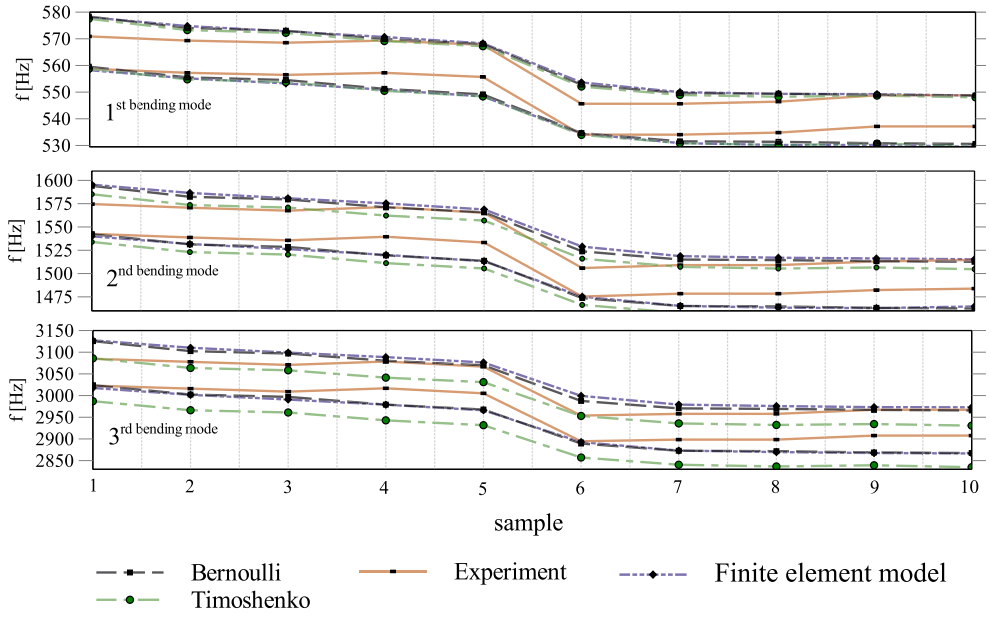

Fig. 7. Values for the first three bending mode natural frequencies with uncertainties for simple beam-like structures; finite element model with two layers, an element edge length of 1 mm and quadratic brick elements with 20 nodes.

processing, and data analysis.

Fig. 7 shows the natural frequencies' uncertainty interval of the first three bending modes for each of the ten specimens. Considering uncertainty intervals, $f_{\min}$ and $f_{\max}$ are the upper and lower limits due to parameter and modeling uncertainties. As Fig. 7 shows, the uncertainty interval of the numerical results based on the Euler–Bernoulli beam theory and the finite element model both envelop the uncertainty interval of the experimental results for each bending mode. This seems physically reasonable, the total uncertainty due to measurement setup, signal processing, and data analysis is smaller than the total uncertainty of these two numerical models when analyzing such simple structures. The deviation ε_B of Euler–Bernoulli models to experimental results are nearly equal with 0.04%, −0.09%, and −0.08% for all three bending modes. The deviation ε_T of the model based on the Timoshenko beam theory significantly increases with the mode order. More precisely values for ε_T are −0.2%, −0.9%, and −1.6% for the first three natural frequencies. Since Timoshenko beam theory extends the Euler–Bernoulli theory by additional shear deformations, the reduced stiffness yields lower natural frequencies. Both ε_B and ε_T underestimate the natural frequency in all bending modes except the first, where ε_B is positive. Regarding the Timoshenko beam theory, its under–performance for evaluating higher bending modes is discussed in Section 4.3. Calculating a relative deviation based on Equation (28) using arithmetically averaged natural frequencies, the finite element model performs well with −0.06%, −0.07%, and −0.05% for the first three bending modes. The uncertainties for FEM are ±10 Hz (1.75%) for the first, ±27 Hz (2.1%) for the second, and ±53 Hz (1.9%) for the third bending modes.

Although the determined material parameters E, ϱ, and ν have a large uncertainty from a practical point of view Fig. 7 shows another interesting aspect as well. That is, out of the 10 samples there are clearly five nearly identical samples in material and geometry within the manufacturing process of ten specimens based on the same tolerances according DIN ISO 2768-1 (m). The relative deviation of the averaged experimentally determined natural frequencies between samples 1–5 and samples 6–10 is 4.0%, 3.9%, and 3.9% for the first three bending modes. This deviation indicates that a high uncertainty in vibration characterization cannot be ruled out for physical structures which are produced in a single unit of production.

The numerical results only show slight deviations compared to experimental results. The idealized boundary conditions are mapped sufficiently accurately within the experimental modal analysis. Performing appropriate measurements, a modeling setup for external fields such as gravity can be omitted in finite element models. Furthermore, suspending the object at the nodal–lines of the analyzed mode is not essential for precisely determining the structure's natural frequencies.

Based on the small deviations observed between simulations and experiments, it is clear that the material parameters E, ϱ, and ν of the beam-like steel structures can be experimentally determined with sufficient precision. The increase in deviation between measurements and numerical results based on the Timoshenko beam theory seems to indicate a decrease in the quality of this analytical solution. The studies conclude that high-order analytical models do not necessarily lead to more accurate solutions for all structures, at the lower frequency range in any case.

6. Conclusions

This paper discussed real dynamic problems involving samples with tolerances similar to those used in production technology. These tolerances comply normally to DIN ISO 2768-1 (m) used for manufacturing processes. Within this work the first three bending modes' natural frequencies of a simple beam-like structure have been determined by experimental modal analysis and numerically by employing Euler–Bernoulli and Timoshenko beam theory in addition to a three–dimensional finite element model. In this analysis, uncertainties of geometrical and numerical parameters have been estimated and integrated into the numerical models using the interval stochastic method. The major concluded points are as follows:

- the developed method achieved an absolute error relative to experimental results by $<0.1\%$ for the first three eigenfrequencies related to bending modes,
- the determined variability of the natural frequencies due to material and geometry uncertainties was around 2%,
- the geometrical uncertainties give rise to larger uncertainties for natural frequencies compared to material uncertainties of beam-like structures, although the material uncertainties are about two times higher than geometrical uncertainties,
- overall relative uncertainties in mesh discretization in FEM were lower than material and geometry,
- the methods employed here show that estimations for the value of the first bending mode are more accurate than higher modes.

Furthermore, this article shows that the Euler–Bernoulli beam theory provides sufficiently accurate results for the natural frequencies of the first three bending modes whereas the results based on the Timoshenko beam theory increasingly deviate for higher bending modes. Furthermore, it shows that results based on a finite element model consisting of 2.70×10^5 degrees of freedom yield the best agreement with the experimental results. Based on the small deviation of the numerical models from the real dynamic behavior, it is reasoned that structural damping can be neglected. Similarly, the way the samples are suspended in the experimental setup, this can also be disregarded in the numerical modeling.

The given experimental parameter identification method based on ultrasonic measurements yields very precise values of three parameters density, Poisson's ratio and Young's modulus, namely, the averaged measurement uncertainties for the ten steel samples are $\pm 0.171\%$, $\pm 3.2\%$, and $\pm 2.3\%$.

Particularly with regard to complex geometries, three–dimensional finite element models provide sufficient accuracy. The study shows that the best choice regarding computational accuracy and effort is a regular mesh with 20–node quadratic brick elements. Finally, and in general, it has been shown here that given the general uncertainties in the manufacturing process and their accurate identification, structural finite element models feature the highest accuracy.

Acknowledgments

The authors acknowledge the financial support of the Bavarian Research Foundation and the fifth author Zayed University Research Grant RIF-16054.

References

[1] R.G. Ghanem, Uncertainty quantification in computational and prediction science, Int. J. Numer. Meth. Eng. 80 (2009) 671–672.
[2] R.J. Bernhard, F.A. Milner, G. Rabbiolo, Vibrations of a beam and related statistical properties, Math. Comput. Model. 34 (2001) 657–675.
[3] Sameer B. Mulani, Uncertainty Quantification in Dynamic Problems with Large Uncertainties, Ph.D. dissertation, Virginia Polytechnic Institute and State University, 2006.
[4] H.Y. Hwang, Identification techniques of structure connection parameters using frequency response functions, J. Sound Vib. 212 (1998) 469–479.
[5] A. Neumaier, Interval Methods for Systems of Equations, Cambridge University Press, Cambridge, 1990.
[6] R.E. Moore, Methods and Applications of Interval Analysis, Society for Industrial and Applied Mathematics, Philadelphia, 1987.
[7] G. Sargent, Verification and validation of simulation models, in: Proceedings of the Winter Simulation Conference, 2005, pp. 53–59. Orlando.
[8] J. Sim, Z. Qiu, X. Wang, Modal analysis of structures with uncertain–but–bounded parameters via interval analysis, J. Sound Vib. 303 (2007) 29–45.
[9] R.P. Broadwater, H.E. Shaalan, W.J. Fabrycky, Decision evaluation with interval mathematics, IEEE Trans. Power Deliv. 9 (1994) 59–65.
[10] M.S. Kompella, R.J. Bernhard, Measurement of the statistical variation of structural-acoustic characteristics of automotive vehicles, in: SAE Technical Paper, vol. 05, SAE International, 1993, pp. 65–81.
[11] R. Li, R. Ghanem, Adaptive polynomial chaos expansions applied to statistics of extremes in nonlinear random vibration, Probabilist. Eng. Mech. 13 (2) (1998) 125–136.
[12] D. Lucor, C.-H. Su, G.E. Karniadakis, Generalized polynomial chaos and random oscillators, Int. J. Numer. Meth. Eng. 60 (3) (2004) 571–596.
[13] K. Sepahvand, S. Marburg, H.-J. Hardtke, Stochastic free vibration of orthotropic plates using generalized polynomial chaos expansion, J. Sound Vib. 331 (1) (2012) 167–179.
[14] S. Marburg, H.-J. Beer, J. Gier, H.-J. Hardtke, R. Rennert, F. Perret, Experimental verification of structural–acoustic modelling and design optimization, J. Sound Vib. 252 (4) (2002) 591–615.
[15] K. Sephavand, S. Marburg, On construction of uncertain material parameter using generalized polynomial chaos expansion from experimental data, in: Procedia IUTAM, vol. 6, 2013, pp. 4–17.
[16] E. Hills, B. Mace, N. Ferguson, Acoustic response variability in automotive vehicles, J. Sound Vib. 321 (1) (2009) 286–304.
[17] M. Stache, M. Guettler, S. Marburg, A precise non-destructive damage identification technique of long and slender structures based on modal data, J. Sound Vib. 365 (2016) 89–101.
[18] K. Sepahvand, S. Marburg, Non-sampling inverse stochastic numerical experimental identification of random elastic material parameters in composite plates, Mech. Syst. Signal Process. 54 (Supplement C) (2015) 172–181.
[19] S.M. Han, H. Benaroya, T. Wei, Dynamics of transversely vibrating beams using four engineering theories, J. Sound Vib. 225 (5) (1999) 935–988.
[20] M. Şimşek, Fundamental frequency analysis of functionally graded beams by using different higher-order beam theories, Nucl. Eng. Des. 240 (4) (2010) 697–705.

[21] Abaqus, Abaqus 6.13 Online Documentation, Dassault Systmes, Providence, RI, USA, 2014.
[22] K.-J. Bathe, Finite Element Procedures, Prentice-Hall, New Jersey, NJ, USA, 1996.
[23] O.C. Zienkiewicz, R.L. Taylor, The Finite Elemente Methode Volume 1: Basic Formulation and Linear Problems, MacGraw-Hill Book Company, New York, 1989.
[24] J. Bonet, R.D. Wood, Nonlinear Continuum Mechanics for Finite Element Analysis, Cambridge University Press, New York, 2008.
[25] B. Szabo, I. Babuška, Finite Element Analysis, John Wiley & Sons, Inc., New York, 1991.
[26] R.J. Astley, Finite Elements in Solids and Structures. An Introduction, GB: Chapman Hall (Springer), London, 1992.
[27] Z. Qiu, S. Chen, H. Jia, The rayleigh quotient iteration method for computing eigenvalue bounds of structures with bounded uncertain parameters, Comput. Struct. 55 (2) (1995) 221–227.
[28] M. Newman, A. Pipano, Fast Modal Extraction in NASTRAN via the FEER Computer Program, NASA. Langley Research Center, 1973, pp. 485–506. NASTRAN: Users' Experiences.
[29] B.N. Parlett, The Symmetric Eigenvalue Problem, Prentice-Hall, New Jersey, NJ, USA, 1980.
[30] K.J. Bathe, E.L. Wilson, Large eigenvalue problems in dynamic analysis, J. Eng. Mech. Div. 98 (1972) 1471–1485.
[31] D.J. Ewins, Modal Testing: Theory and Practice, Research Studies Press, Letchworth, Hertfordshire, England, 1984.
[32] ISO 7626-1:2011, Methods for the Experimental Determination of Mechanical Mobility; Parts 1-5, International Organisation for Standardization, Switzerland, 1994.
[33] J. Achenbach, Wave Propagation in Elastic Solids, Ser. North-Holland Series in Applied Mathematics and Mechanics, Elsevier Science, 2012.
[34] J. Hislop, J. Krautkrämer, H. Krautkrämer, W. Grabendörfer, R. Frielinghaus, W. Kaule, L. Niklas, U. Opara, U. Schlengermann, H. Steiger, et al., Ultrasonic Testing of Materials, Springer Berlin Heidelberg, 2013.
[35] A. Labuschagne, N.F.J. van Rensburg, A.J. van der Merwe, Comparison of linear beam theories, Math. Comput. Model. 49 (1-2) (2009) 20–30.
[36] P. Langer, K. Sepahvand, S. Marburg, Uncertainty quantification in analytical and finite element beam models using experimental data, in: A. Cunha, E. Caetano, P. Ribeiro, G. Müller (Eds.), Proceedings of the 9th International Conference on Structural Dynamics, EURODYN 2014, 2014. Porto, Portugal.
[37] P. Langer, K. Sepahvand, M. Krause, S. Marburg, Experimentally uncertainty quantification in numerical and analytical beam models, in: J. Davy, C. Don, T. McMinn, L. Dowsett, N. Broner, B. Marion (Eds.), Proceedings of Inter-noise 2014, vol. 249, no. 5, Institute of Noise Control Engineering, 2014, pp. 2357–2366.
[38] P. Langer, M. Maeder, C. Guist, M. Krause, S. Marburg, More than six elements per wavelength: the practical use of structural finite element models and their accuracy in comparison with experimental results, Submission for special issue on numerical methods for vibro-acoustics and aeroacoustics to J. Comput. Acoust. 25 (04) (2017) 1750025.